Core-shell Silica-coated Iron Oxide Nanoparticles for Magnetic Hyperthermia

Yousaf Iqbal, Hongsub Bae, Sungwook Hong, and Ilsu Rhee*

Department of Physics, Kyungpook National University, Daegu, Korea, *ilrhee@knu.ac.kr

ABSTRACT

We report the synthesis and characterization of silica-coated iron oxide nanoparticles with a core-shell structure for magnetic hyperthermia. The nanoparticles of silica-coated iron oxide were synthesized using the reverse micelle method. The coating of the silica was performed simultaneously with the synthesis of the nanoparticles. The as-synthesized silica-coated iron oxide nanoparticles exhibited superparamagetic properties with a saturation magnetization of 48.8 emu/g. The inductive heating ability of the nanoparticles dispersed in water with a concentration of 20 mg/ml was investigated in a 1.03-kA/m, 260-kHz alternating magnetic field. The results revealed a heat release of up to 139 W per one gram of iron, demonstrating the potential application of the nanoparticles in magnetic hyperthermia.

Keywords: Silica-coated iron oxide nanoparticles, Magnetic hyperthermia, Specific absorption rate (SAR).

1. INTRODUCTION

Magnetic nanoparticles have attracted substantial attention in recent years owing to their practical applications, such as ferrofluids [1], magnetic recording [2], drug delivery [3], MRI contrast agents [4, 5], and magnetic hyperthermia treatment [6]. Among the magnetic nanoparticles, iron oxide (magnetite, Fe_3O_4) is one of the important spinel-structured ferrites, which with its superparamagnetic properties, makes it useful for biomedical applications, including magnetic hyperthermia.

Hyperthermia treatment is a cancer therapy in which tumor tissues are killed by increasing their temperature up to 42 ℃. Tissues can be heated by injected magnetic nanoparticles in response to an alternating magnetic field. The dissipation of heat in magnetic nanoparticles in an alternating magnetic field is caused mainly by Néel and Brownian relaxation losses [7, 8]. The heating ability of magnetic nanoparticles depends on the particle concentration, duration of exposure to the alternating magnetic field, and tissue characteristics [9, 10].

Magnetic nanoparticles tend to agglomerate after being injected intravenously to form clusters in the blood because of their high surface-to-volume ratio and surface energy. In addition, due to the activation of opsonization (clearance mechanism) by the reticuloendothelial system (RES), the nanoparticles are bound with plasma proteins before reaching the target area of the body. Recently, silica has been widely used as a coating material because of its excellent biocompatibility and ease of surface functionalization with various functional groups owing to the existence of abundant silanol groups on the silica layer. Also, silica is able to screen the magnetic dipolar attraction between the magnetic nanoparticles, facilitating their dispersion in liquid media.

In this study, silica-coated iron oxide nanoparticles were synthesized by the reverse micelle method to evaluate their applicability in magnetic hyperthermia. The structural and magnetic properties of the nanoparticles were measured by various analytical tools. These results indicated superparamagnetic behavior and a self-heating mechanism in the applied alternating magnetic field.

2. EXPERIMENTAL

The synthesis of the silica-coated iron oxide nanoparticles was based on the procedure reported by Ahmad et al. [11] and J. Lee et al. [12]. In brief, a water-in-oil system was obtained by the following procedure: 3.5 g of sodium dodecylbenzenesulfonate (NaDBS) was dissolved in 30 ml of xylene (isomers plus ethylbenzene, 98.5%) to form a transparent solution under ultrasonication. Under vigorous mechanical stirring at 500 rpm, 1.8 ml of an aqueous solution containing stoichiometric amounts of iron (II) chloride tetrahydrate ($FeCl_2$-$4H_2O$, 99%) and iron (III) nitrate nanohydrate ($Fe(NO_3)_3$-$9H_2O$, 98%) was added to this mixture. The transparent solution turned milky white upon the addition of the aqueous solution. The resultant water-in-oil system was continuously stirred for about 16 to 18 h, followed by additional stirring for 1 h under nitrogen protection. After stirring, the system was heated to 90 ℃ at a rate of 2 ℃/min and 1 ml of hydrazine (34 wt% water solution) was added. The resultant system was kept at 90 ℃ for 3 h and then cooled down to 40 ℃ over about 1.5 h. During this process, iron oxide (Fe_3O_4) nanoparticles were formed inside the mini reactors of the reverse micelle (water-in-oil) system. To coat the nanoparticles with silica, 4 ml of TEOS (tetraethyl orthosilicate) was added to the resultant solution at 40 ℃ and stirred for about 6 h at 500 rpm. The silica-coated iron oxide nanoparticles were separated from the oil phase by using acetone and subsequent centrifugations at 13,000 rpm. All the chemicals were purchased from Sigma-Aldrich, analytical grade and used without any further purification. For further measurements, the product was dried at room temperature.

The morphology and particle size distribution of the silica-coated nanoparticles were analyzed by transmission electron microscopy (TEM; H-7600, Hitachi Ltd.). The crystal structure of the silica-coated iron oxide nanoparticles was investigated by using X-ray diffraction (XRD; X'pert PRO, PANalytical). Analysis of the bonding of the silica on the surface of the iron oxide was performed by using Fourier transform infrared spectroscopy (FTIR, Nicolet 380, Thermo Scientific USA). The magnetic measurement was carried out using a vibrating sample magnetometer (VSM, Lakeshore 7400). The heating effects of nanoparticles dispersed in water were measured using an induction heating system (Osung High tech, OSH-120-B) with a frequency of 260 kHz and a magnetic field strength of 1.03 kA/m. The temperature was measured with a CALEX infrared thermometer (PyroUSB CF, Calax Electronics Limited).

3. RESULTS AND DISCUSSIONS

Figure 1 shows TEM images of the core-shell nature and spherical morphology of the silica-coated iron oxide nanoparticles. The visible dark spots represent the iron oxide (core) and the translucent region around the iron oxide is the silica coating (shells). It can also be seen from the TEM images that the nanoparticles were nearly mono-dispersed with an average diameter of 17 nm, and a silica shell thickness of about 4 nm.

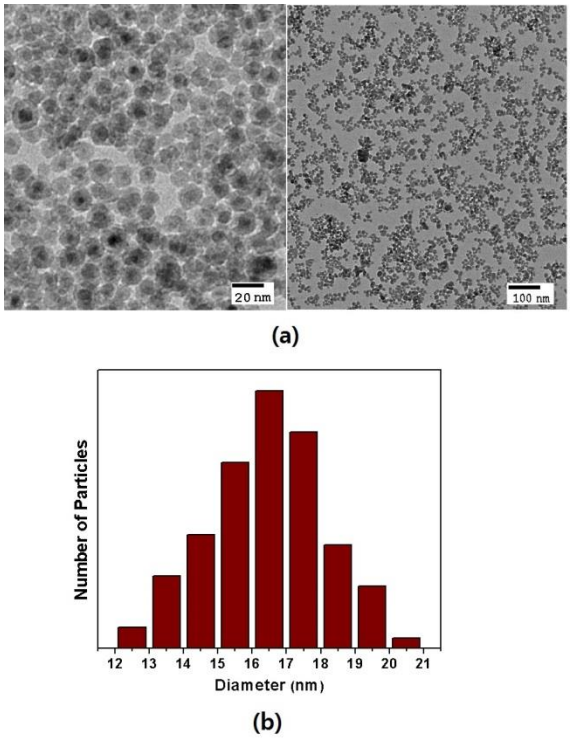

Figure 1. (a) TEM images of core-shell silica-coated iron oxide nanoparticles (b) Particle size distributions for one hundred particles obtained from a TEM image.

The crystal structure of the silica-coated iron oxide nanoparticles was investigated by powder XRD measurements. Figure 2 shows XRD patterns of the silica-coated iron oxide nanoparticles with six Bragg diffraction peaks at 30.09, 35.50, 42.80, 53.40, 57.49, and 62.69° of 2θ, which correspond to the (220), (311), (400), (422), (511), and (440) crystal planes, respectively, matching those observed in the spinel ferrite [13].

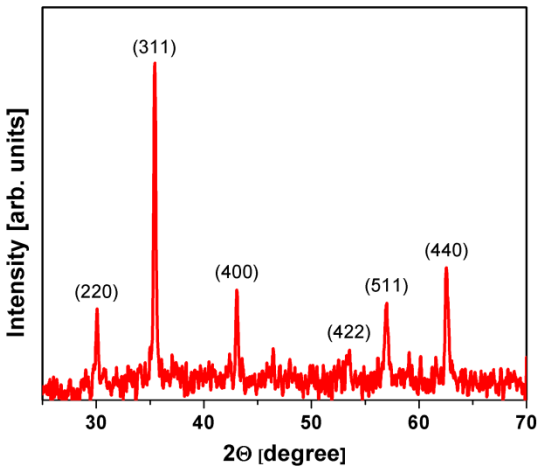

Figure 2. XRD pattern of silica-coated iron oxide nanoparticles. The indices of the crystal planes in the figure match those of the cubic spinel structure.

The silica on the surface of the iron oxide nanoparticles was investigated by FTIR in the range of 400 to 4,000 cm^{-1}. Figure 3 shows the absorption bands at around 3,410 and 1,633 cm^{-1} corresponding to the stretching and vibration modes of O–H groups present at the surface of the sample [14, 15]. In addition, the absorption bands at 452 and 1,103 cm^{-1} are due to the Si–O–Si stretching vibrations and Si–O bending vibrations, respectively, while the band at 804 cm^{-1} is due to SiO_4 ring vibrations [16]. The absorption band at 955 cm^{-1} is assigned to the Si–O–H stretching vibration [17]. The above results clearly confirm the presence of biocompatible silica on the surface of the iron oxide nanoparticles.

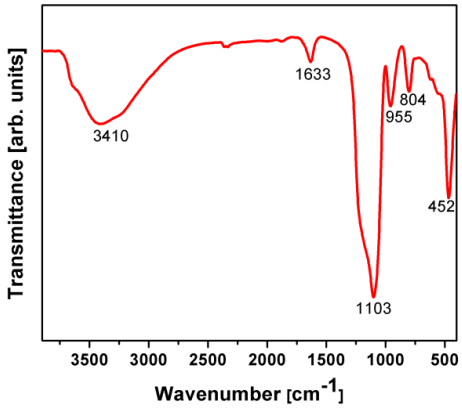

Figure 3. FTIR spectra of silica-coated iron oxide nanoparticles.

The magnetic properties were measured by using a VSM. Figure 4 shows the magnetization as a function of magnetic field at room temperature. The absence of the remanence and coercivity indicates the characteristic superparamagetic behavior at room temperature. The saturation magnetization was measured to be 48.8 emu/g, comparable to the value of the bulk iron oxide [18]. Superparamagetic behavior, the lack of any residual magnetization after the removal of the external magnetic field, is preferred for biomedical applications [19].

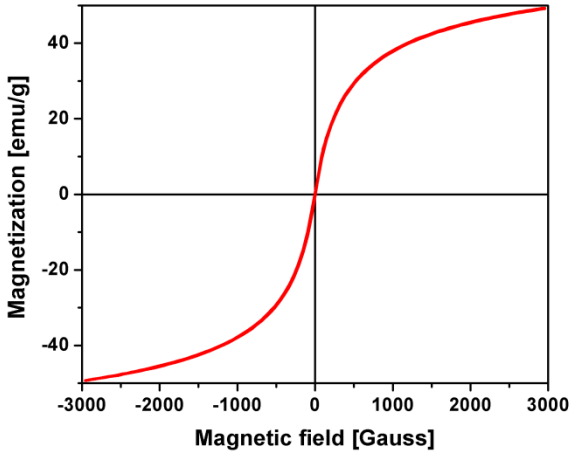

Figure 4. Hysteresis curve of silica-coated iron oxide nanoparticles at room temperature.

Figure 5(a) shows a plot of temperature rise as a function of time for the silica-coated iron oxide nanoparticles dispersed in water with concentrations of 20, 15, and 10 mg/ml in a 1.03-kA/m, 260-kHz alternating magnetic field. The heat dissipation ability of the silica-coated iron oxide nanoparticles can be characterized by specific absorption rate (SAR) values, defined by the amount of heat dissipated per unit mass of iron in the ferrofluid solution [20, 21]

$$SAR\left(\frac{W}{g}\right) = C_p\left[\frac{1}{m_{Fe}}\right]\frac{\Delta T}{\Delta t} \quad , \qquad (1)$$

where C_p is the specific heat capacity of the buffer (4,186 J/kg·K for water), m_{Fe} is the final mass fraction of iron in the sample obtained from ICP (3.388 g/L, 2.541 g/L, and 1.694 g/L for the 20, 15, and 10 mg/ml samples, respectively) and $\frac{\Delta T}{\Delta t}$ is the initial slope over the first 60 s of the heating curve (figure 5a).

For the 20, 15, and 10 mg/ml samples, the SAR values calculated by using equation (1) were 139.62, 126.85, and 86.49 W/g, respectively. The temperature for the 20 mg/ml sample reached the saturation temperature of about 50 ℃ in 750 s, crossing the effective and appropriate temperature of 42– 45 ℃ for the localized hyperthermia treatment of cancer in about 300 s. This heating is caused by the relaxation processes of particle's magnetic moment in an alternating magnetic field. Two distinct mechanisms are responsible for the relaxation process: i) the Brownian relaxation loss due to the friction between the fluid and rotating nanoparticles and ii) the Néel relaxation loss due to the delay of the magnetic moment reversal across the anisotropy barrier [22]. As expected, the SAR values decrease with a decrease in the nanoparticle concentration, as shown in Fig. 5(b). As SAR is a colligative property that depends on the number of particles, an increasing concentration would result in more magnetic particles, resulting in high SAR values.

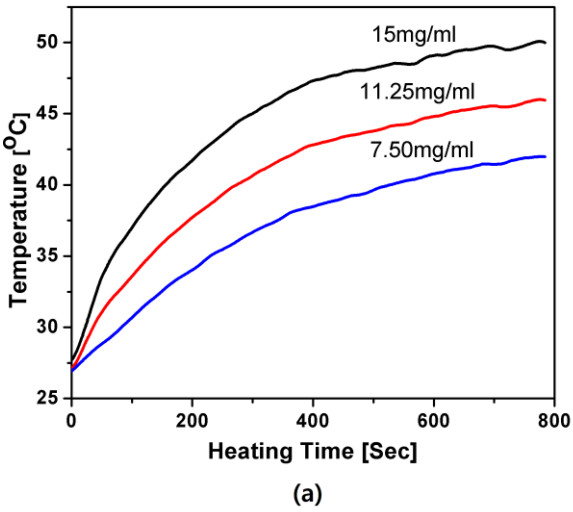

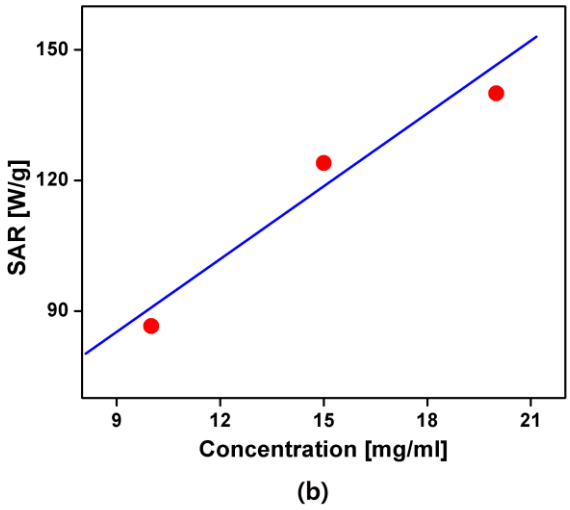

Figure 5.(a) Heating effect of the dispersions of silica-coated iron oxide nanoparticles with concentrations of 20, 15, and 10 mg/ml under a 1.03-kA/m, 260-kHz alternating magnetic field. (b) Concentration dependence of specific absorption rate (SAR) values.

IV. CONCLUSIONS

Mono-dispersed silica-coated iron oxide (Fe_3O_4) nanoparticles were fabricated by using the reverse micelle method. The silica-coated nanoparticles were spherical in shape and near-mono-dispersed in size, with an average

diameter of 17 nm. The superparamagnetic behavior of nanoparticles was observed by a hysteresis curve. This behavior caused the nanoparticles to heat up in an alternating magnetic field as a result of the Néel and Brownian processes. The 10, 15, and 20 mg/ml samples showed a sufficient heating effect, which is higher than that of conventional iron-oxide nanoparticles, and therefore, can be efficiently used for practical hyperthermia applications.

ACKNOWLEDGEMENTS

This work was supported by the National Research Foundation of Korea (2010-0021315).

REFERENCES

[1] K. Raj, B. Moskowitz, and R. Casciari, J. Magn. Magn.Mater. 149, 174, 1995.
[2] A.H. Lu, E.L. Salabas, and F. Schüth, Angew. Chem., Int. Ed. 46, 1222, 2007.
[3] E. Ruiz-Hernández, A. Baeza, and M. Vallet-Regí,ACSNano, 5, 1259, 2011.
[4] T. Ahmad, H. Bae, S. Hong, Y. Chang, S. Jin, and I. Rhee, J. Nanosci.Nanotech.12, 5132, 2012.
[5] T. Ahmad, Y.Iqbal, H.Bae, I. Rhee, S. Hong, Y. Chang, and J. Lee, J. Korean Phys. Soc. 62, 1696, 2013.
[6] R. Hergt and S. Dutz, J. Magn. Magn.Mater. 311, 187, 2007.
[7] R. E. Rosensweig, J. Magn. Magn. Mater. 252, 370, 2002.
[8] L. Y. Zhang, H. C. Gu, and X. M. Wang, J. Magn. Magn. Mater. 311, 228, 2007.
[9] S. A. Shah, A. Majeed, K. Rashid, and S. Awan, Mater. Chem. Phys 138, 703, 2013.
[10] C. S. S. R. Kumar and F. Mohammad, Adv. Drug Deliv. Rev. 63, 789, 2011.
[11] T. Ahmad, I. Rhee, S. Hong, Y. Chang, and J. Lee, J. Korean Phys. Soc. 56, 1545, 2010.
[12] J. Lee, Y. Lee, J.-K. Youn, H.-B. Na, T. Yu, H. Kim, S.-M. Lee, Y.-M. Koo, J.-H, Kwak, H.-G. Park, H.-N. Chang, M. Hwang, J.-G. Park, J. Kim, and T. Hyeon, Small, 4, 143, 2008.
[13] M. Abbas, M. Takahashi, and C. Kim, Journal of Nanoparticle Research, 15, 1354 , 2013.
[14] L. Chen, Z. Xu, H. Dai, and S. Zhang, J. Alloys Comp. 497, 221, 2010.
[15] S. Bruni, F. Cariati, M. Casu, A. Lai, A. Musinu, G. Piccaluga, and S. Solinas, Nanostruct. Mater. 11, 573, 1999.
[16] J. Lewandowska-Łan´cucka, M. Staszewska, M. Szuwarzynski, M. Kepczynski, M. Romek, W. Tokarz, A. Szpak, G. Kania, and M. Nowakowska, J. Alloys Comp. 586, 45, 2014.
[17] B. Mojić, K. P. Giannakopoulos, Z. Cvejić, and V. V. Srdić, Ceramics International, 38, 6635, 2012.
[18] W. Wu, Q. He, and C. Jiang, Nanoscale Res. Lett. 3, 397, 2008.
[19] S. Laurent, S. Dutz, U. O. Häfeli, and M. Mahmoudi, Adv. Colloid Interface Sci. 166, 8, 2011.
[20] A. Cervadoro, M. Cho, J. Key, C. Cooper, C. Stigliano, S. Aryal, A. Brazdeikis, J. F. Leary, and P. Decuzzi, ACS Appl. Mater. Interfaces, 6 1, 2939, 2014.
[21] P. Guaridia, R. D. Carato, L. Lartigue, C. Wilhelm, A. Espinosa, M. Garcia-Hernandez, F. Gazeau, L. Manna, and T. Pellegrino, J. Am. Chem. Soc., 6, 3080 (2012).
[22] R. Hergt, S. Dutz, R. Müller, and M. Zeisberger, J. Phys. Condens. Matter 18, S2919, 2006.